JOURNAL OF EXPERIMENTAL AND THEORETICAL PHYSICS, 2024, Vol. 165, No. 4, pp. 550–562

ORDER, DISORDER AND PHASE TRANSITIONS IN CONDENSED MEDIA

STUDY OF THE CORRELATION BETWEEN THE TOPOLOGICAL PHASE TRANSITION, AXION-LIKE STATE AND MAGNETOELECTRIC EFFECT IN ANTIFERROMAGNETIC TOPOLOGICAL INSULATOR $MnBi_2Te_4$

© 2024 A. M. Shikin[a,*], T. P. Estyunina[a], A. V. Eryzhenkov[a], N. L. Zaitsev[b], A. V. Tarasov[a]

[a] *Saint Petersburg State University, 198504, Saint Petersburg, Russia*

[b] *Institute of Molecule and Crystal Physics, Ufa Federal Research Centre of the Russian Academy of Sciences, 450075, Ufa, Russia*

**e-mail: ashikin@inbox.ru*

Received November 14, 2023
Revised December 04, 2023
Accepted December 04, 2023

Abstract. Density functional theory calculations have been performed to demonstrate the possibility of implementing a topological phase transition (TPT) from topological to trivial state and the connection of this transition with the formation of an axion-like state in an antiferromagnetic topological insulator $MnBi_2Te_4$ through analysis of changes in the electronic and spin structures of topological surface states (TSS) and the energy gap value at the Dirac point (DP) when varying the strength of spin-orbit interaction. The analysis showed that this TPT corresponds to the minimum of the energy gap opened at the DP and is characterized by the p_z^+-states of Bi and p_z^--states of Te inversion of with different parity at the edges of the formed energy gap, which corresponds to the sign change of the energy gap in the TPT region between topological and trivial phases. At the transition point, there is an inversion of out-of-plane spin polarization for the states of the lower and upper parts of the Dirac cone and spatial redistribution of states forming TSS between the surface and bulk. The TPT occurs without complete closure of the energy gap with a "jump" through zero and formation of a non-zero energy gap value, which we associate with the formation of an axion-like state caused by the non-trivial interrelation of non-magnetic (spin-orbit) and magnetic interactions at the boundary between topological and trivial phases for a system with parameters close to TPT. A comprehensive representation of such intercoupling in the TPT region is proposed, where the axion term changes between quantized values π and 0, characteristic for topological and trivial phases, leading to their intercoupling in the TPT region and determining the non-zero energy gap at the DP. Application of an electric field perpendicular to the surface of the system in the TPT state leads to changes in electronic and spin structures and transition from topological to trivial state of the system and vice versa when changing the direction of the applied field, demonstrating the possibility of implementing the topological magnetoelectric effect in the TPT region.

Keywords: *magnetic topological insulator, topological phase transition, density functional theory, axion-like state, topological surface state*

DOI: 10.31857/S004445102404e096

1. INTRODUCTION

One of the most interesting features of magnetic axion topological insulators (TI), the most prominent representative of which is the recently synthesized antiferromagnetic (AFM) TI $MnBi_2Te_4$, is the topological quantum magnetoelectric (ME) effect, the implementation of which is determined by the so-called axion term θ, which separates topological and trivial insulators and determines many unique properties of TI (see, for example, reviews [1–5]). Initially, the concept of axion (and axion field) came to condensed matter physics [1–12] from elementary particle physics and topological field theory [13, 14] to describe the ME response (static and dynamic) to external electromagnetic influence through the introduction

of an additional axion term in the system's Lagrangian

$$S_\theta = \frac{\theta}{2\pi}\frac{e^2}{\hbar c}\int d^3x dt \mathbf{E}\cdot\mathbf{B},$$

defined by a pseudoscalar field θ, the value of which can vary depending on the type of system symmetry [1–5]. Here

$$\frac{e^2}{\hbar c} = \alpha$$

is the fine structure constant, **E** and **B** are electric and magnetic fields. In the presence of time reversal symmetry and spatial symmetry, the axion term θ takes a quantized value $\theta = \pi$ for topological media and $\theta = 0$ in trivial media [1–5], thereby introducing a difference in ME response between topological and trivial media and determining the quantization of ME effect, as well as the possibility of realizing the quantum anomalous Hall effect in magnetic TI. At the boundary between topological and trivial media (vacuum is considered as a trivial insulator) θ varies within the range from π in TI to 0 in vacuum. On the other hand, currently the concept of axion (α) is considered more broadly, including as a result of interaction between fermions and antifermions of opposite chirality [15]

$$f + f^* \to \alpha,$$

which is accompanied by the opening of a band gap in the formed dispersion relations (i.e., the appearance of mass) during such interactions, mainly between topological and trivial phases. Or rather the concept of axion can be considered as a result of interaction between ordinary and virtual (dark) photons ($\gamma + \gamma^* \to \alpha$) that represent massless fermions (with violation of time reversal symmetry and parity) which determine the formation of axion mass and thereby defines significant interest in the problem of axion in cosmology, astrophysics and superstring theory [15–18]. At the same time, axion as a hypothetical particle (with small mass) is also a possible component in interaction with dark matter [17, 18]. Moreover, in many models, to describe the axion field, a complex field $\Phi = \chi e^{i\theta}$ is introduced, which is characterized by a non-zero vacuum expectation value (axion potential), depending on the chiral symmetry of the system. In condensed matter physics, the concept of axion was introduced precisely based on the similarity of ME response in TI under external electromagnetic influence.

Based on these correlations, in condensed matter physics, the concept of an axion insulator was introduced as a magnetic TI characterized by opposite out-of-plane spin orientation (perpendicular to the TI surface) on opposite surfaces. This type of axion insulator is characterized by a quantized topological ME response (proportional to $\pm(1/2)e^2/\hbar c$) and the corresponding quantized value of surface conductivity, which is determined by the quantized value of the axion term $\theta/2\pi$ (at $\theta = \pi$) in the corresponding expression for the Lagrangian [3, 4, 6–12, 19–22]. In this case, it is precisely the change of θ to π at the boundary between topological and trivial media (i.e., at the θ-boundary) that ensures the realization of the topological quantized ME effect and the quantum half-integer Hall effect at this θ-boundary, i.e., on the surface of such an axion insulator.

Initially, the idea of an axion insulator was intensively developed in works [19–22], where the axion insulator was built on the basis of a layered topological structure in which layers of Cr- and V-doped magnetic TI $(Bi, Te)_2Te_3$ with different coercive forces and opposite orientation of magnetic moments interacted through a layer of non-magnetic TI. For this type of axion insulator the zero-plateau quantum anomalous Hall effect was first demonstrated, and the realization of the topological ME effect was proposed. However, recently, a new type of intrinsic magnetically ordered AFM TI with natural opposite orientation of magnetic moments in neighboring magnetic layers has been synthesized, which can serve as a promising platform [23–32] for implementing axion-like state and studying it in a more natural and optimal way. Currently, there exists a whole series of works analyzing the possibility of implementing the axion insulator state and dynamic axion effect in compounds based on $MnBi_2Te_4$, as well as TI from the family of $(MnBi_2Te_4)_m(Bi_2Te_4)_n$ and proposed new compounds like $MnBi_2Te_5$ or $MnBi_6Te_{11}$ [8, 10–12], where the possibility of modulating AFM interaction and the strength of spin-orbital (SO) coupling was shown, leading to effective formation of spin AFM fluctuations and corresponding dynamic modulation of the axion field $\delta\theta(r,t)$, which implies the possibility of more detailed study of axion state properties in condensed matter physics.

Despite the fact that these compounds, including similar compound $Mn_2Sb_2Te_5$ [33], are characterized by a more complex structure

(for $Mn_2Bi_2Te_5$ and $Mn_2Sb_2Te_5$ with two layers of Mn atoms in the unit cell [12, 33]), they are also axion AFM insulators in which dynamic axion effect can be realized, possibly even to a greater extent [10], due to higher concentration of magnetic Mn atoms in the unit cell.

AFM TI $MnBi_2Te_4$ is a layered compound consisting of septuple layer blocks (SL) Te-Bi-Te-Mn-Te-Bi-Te, separated by van der Waals intervals [23–32, 34–37]. The Mn atoms in the magnetic layer within each formed SL are located in one plane and are coupled by ferromagnetic interaction, while the interaction between neighbouring SLs and corresponding magnetic Mn-layers has an AFM character [23–32, 34]. For AFM TI, despite the violation of both time-reversal symmetry and spatial symmetry (and parity), their combination in the case of layer-by-layer AFM ordering preserves the topological invariant [23–26]. It was shown that this AFM TI is indeed an axion insulator with opposite orientation of magnetic moments on opposite surfaces (provided that the number of layers comprising the system is even), where each surface is characterized by a contribution to conductivity equal to half of the conductivity quantum, but with opposite signs $\pm(1/2)e^2/\hbar c$, thus compensating each other, which is the basis of the zero-plateau quantum anomalous Hall effect and the necessary condition for the realization of the axion state, as well as the possibility of effective implementation of the dynamic axion field (effect) [1–5, 8–12, 19–22].

It should be noted that the axion idea was initially introduced and studied in condensed matter physics specifically during the analysis of possible manifestation of the dynamic axion effect in magnetic TI [8–12], i.e., the excitation of dynamic axion field under electromagnetic radiation (in the presence of magnetic field), which can be experimentally detected through the excitation of axion polariton [8]. In this context, the concepts of static (θ_0) and dynamic ($\delta\theta$) parts of the axion term (axion field) were introduced: $\theta(r,t) = \theta_0 + \delta\theta(r,t)$. The static part can be considered as a dimensionless pseudoscalar parameter (or pseudoscalar axion field). The dynamic part, which is time-dependent, is caused by the change in θ, created by external influence (external electromagnetic field combined with applied magnetic field breaking time-reversal symmetry), which leads to the modulation of θ relative to $\theta_0(r) = \pi$ [1, 4, 8–12]. As a result of the conducted research, it was shown that the most effective implementation of the dynamic axion effect can be achieved when the system is characterized by a minimal energy gap value, primarily determined by the change in the strength of SO-coupling, and is parametrically in the region of topological phase transition (TPT) from topological to trivial state, when θ changes from π to 0. At the TPT point, the energy gap value passes through a minimum with inversion of states of different parity at the energy gap edges, i.e., with a change in the sign of the formed energy gap [1–4, 8–12].

Based on the concepts of the axion (or axion-like state) mentioned above, as a result of the interaction between two Dirac fermions with linear dispersion of opposite chirality, $f + f^* \rightarrow \alpha$, we will search for and analyze the axion-like state realized in AFM TI $MnBi_2Te_4$, by analyzing changes in the electronic and spin structures of topological surface states (TSS) as states with initial linear dispersion in the region of TPT from topological to trivial state (i.e., with changes in $\theta = \pi \rightarrow 0$) and changes in the energy gap value at the DP (when modulating the strength of the SO-coupling), caused by the intercoupling (as will be shown below) of non-magnetic (SO) and magnetic interactions at the θ-boundary between topological and trivial phases. The analysis will be carried out based on calculations of electronic and spin structures using density functional theory in slabs of various thicknesses while modulating the strength of the SO-coupling λ_{SOC} in the TPT region, where the energy gap value at the DP reaches its minimum, and the energy gap changes its sign (due to inversion of states with different parity (p_z^+-states of Bi and p_z^--states of Te)) during the system's transition from topological to trivial state.

Special attention is paid to investigating the conditions for achieving the minimum of the energy gap value at the DP, inversion of state contributions at the edges of the forming energy gap, and changes in spin structure at the minimum value of energy gap, as well as analyzing parameters that can affect the value of the energy gap in the region of its minimum value when modifying the strength of λ_{SOC}. At the end of the work, results of calculations on the influence of electric field of opposite direction applied perpendicular to the surface and the possibility of field- stimulated controlled transition between topological and trivial states of the system is presented.

2. RESULTS AND DISCUSSION

In previous publications devoted to the study of electronic structure $MnBi_2Te_4$, it was shown that for various samples of this TI, it is possible to form both a large energy gap at the DP (80–90 meV from theoretical estimates [23, 25, 26] or 50–60 meV from experimental studies [27–32, 34]), and a small EG (up to 5–10 meV and lower down to gapless dispersions) opening in the TSS structure [35–37]. It was shown that if the strength of the effective SO-interaction is modulated (decreased) λ_{SOC} in the initial AFM TI $MnBi_2Te_4$, this will lead to a significant change (decrease) in the bulk band gap in such a model system [25, 26], up to reinversion of p_z^+- of Bi and p_z^--states of Te at the band edges and the system's transition from topological to trivial state. The inversion point of these states corresponds exactly to the TPT point. Similar changes with variation of λ_{SOC} also occur (as we will be show later) for the energy gap in the TSS structure at the DP, see also [34]. Importantly, it is the minimum of the bulk band gap (as we noted above), as well as the energy gap at the DP (as will be shown below) that corresponds most closely to the conditions for realizing an axion-like state at the boundary between topological and trivial phases.

2.1. Influence of modulation of the SO-coupling in AFM TI $MnBi_2Te_4$ on changes in the electronic structure of TSS and modulation of the value of the energy gap at the Dirac point. Role of topological phase transition

Fig. 1a1 schematically presents a diagram of changes in the energy position of levels that form the valence band and conduction band (with variation of SO-coupling strength and without λ_{SOC}), as well as the corresponding inversion of p_z^+ -states of Bi and p_z^--states of Te, which are localized at the edges of the formed bulk band gap. This $MnBi_2Te_4$ diagram allows qualitative prediction of changes in the value and sign of the p_z^+-states of Bi and p_z^--states of Te formed bulk band gap that will occur during the transition between topological and trivial states of the system with variation of λ_{SOC} in the bulk of the $MnBi_2Te_4$ (taken from work [26]). The signs "+" and "-" correspond to the parity of states. The energy distributions of the electronic of Bi at the edges of the formed band gap are shown with and without SO-interaction throughout the entire bulk of the crystal (taken from [26]). The presented diagram shows that if the strength of the λ_{SOC} in the crystal is reduced from the value characteristic of the topological phase $\lambda_{SOC} = 1$ to zero value ($\lambda_{SOC} = 0$), then at certain values of λ_{SOC} one can reach a point characterized by the minimum band gap value and inversion of p_z^+-states of Bi and p_z^-- states of Te with different parity, forming the band gap edges, which will correspond to TPT between trivial and topological states of the system. This work will analyze in more detail the corresponding changes in the dispersion dependence of TSS for $MnBi_2Te_4$ with changes in the strength of λ_{SOC} for slabs of different thickness (from 6 to 24 SLs). In practice, the possibility of changing the strength of λ_{SOC} is assumed when replacing (fully or partially)heavy metal atoms (Te, Bi) with lighter element (Se, S, Sb). Works [38–40] analyze changes in the electronic structure of compounds $MnSb_2Te_4$, $MnBiSe_4$ and others, where Bi and Te atoms are replaced with Sb and Se atoms. The results show that these compounds, due to the smaller strength of atomic SO-interaction of substituting atoms, are indeed closer to the TPT region and, depending on structural parameters and applied pressure, can transform from the AFM TI phase to trivial or ferromagnetic phase. Moreover, work [41] shows that gradual replacement of Te atoms with Se atoms indeed leads to modulation of the band gap size and TPT to trivial state for compounds with stoichiometry close to $MnBi_2Te_2Se_2$.

Fig. 1a2–a5 shows the changes in the dispersion dependence of TSS (and corresponding changes in the energy gap value at the DP), as well as the nearest states of the valence band and conduction band for a slab with thickness of 18 SLs under variation of λ_{SOC} (relative to the initial value λ_{SOC}, characteristic for $MnBi_2Te_4$, taken as 1) for atoms in the calculated slab. Similar dependencies of the changes of the energy gap value at the Dirac point for the calculated slab thickness of 12 SLs are presented in work [41], which differ in the achievable energy gap value at the DP. The presented results show that when λ_{SOC} decreases below $\lambda_{SOC} = 1$, the value at the DP also decreases and reaches a minimum. After passing the minimum point, the energy gap at the DP value begins to increase again. This minimum in the energy gap (as we will

show below) corresponds to the TPT region between the trivial and topological states of the system.

Figs. 1a6–a9 show in more detail the dispersion dependence of TSS at the point of minimum energy gap value at the DP for all thicknesses of the calculated slab (6, 12, 18, 24 SLs), and Fig. 1a10 shows for comparison the corresponding changes in the energy gap value under variation of λ_{SOC} (both above and below the region of the minimal energy gap value) for all thicknesses of the calculated slab. The calculated values of minimal energy gap value at the DP for different slab thicknesses are 19 meV for 6 SLs, 9.5 meV for 12 SLs, 6.5 meV for 18 SLs, and 4.2 meV for 24 SLs. The color scheme in the presented dispersions in Fig. 1a1–a5 and 1a6–a9 corresponds to the difference between contributions of the Te p_z^--states and Bi p_z^+-states in the formed electronic structure. Red (blue) color corresponds to the prevalence of contribution of the Te p_z^--states (Bi p_z^+-states). Analysis of the presented contributions shows that both TSS at the edges of the Dirac energy gap and states at the edges of the bulk band gap demonstrate clear inversion of contributions of p_z^-- states Te (p_z^+-states Bi) in the region of point Γ during transition between topological and trivial states of the system. Such inversion, on one hand, confirms the presence of TPT from topological to trivial state (and vice versa) with changes in λ_{SOC}, and on the other hand, indicates the inversion of energy gap sign during TPT. The trivial state of the system corresponds to positive energy gap, while topological phase corresponds to negative energy gap [1, 4, 10–12, 34, 42, 43].

The above-noted changes in energy gap value for different slab thicknesses could be attempted to explain by the influence of correlation effects between TSS at slab edges (finite size effects of the slab). It is well known that decreasing the calculated slab thickness below certain limits can lead to increased correlation effects between states at slab edges [10, 44, 45]), which may be accompanied by an increase in the calculated value of the energy gap. However, it is considered that the influence of correlation effects manifests significantly for slab thicknesses less than 4–6 SLs, while for slab thickness more than

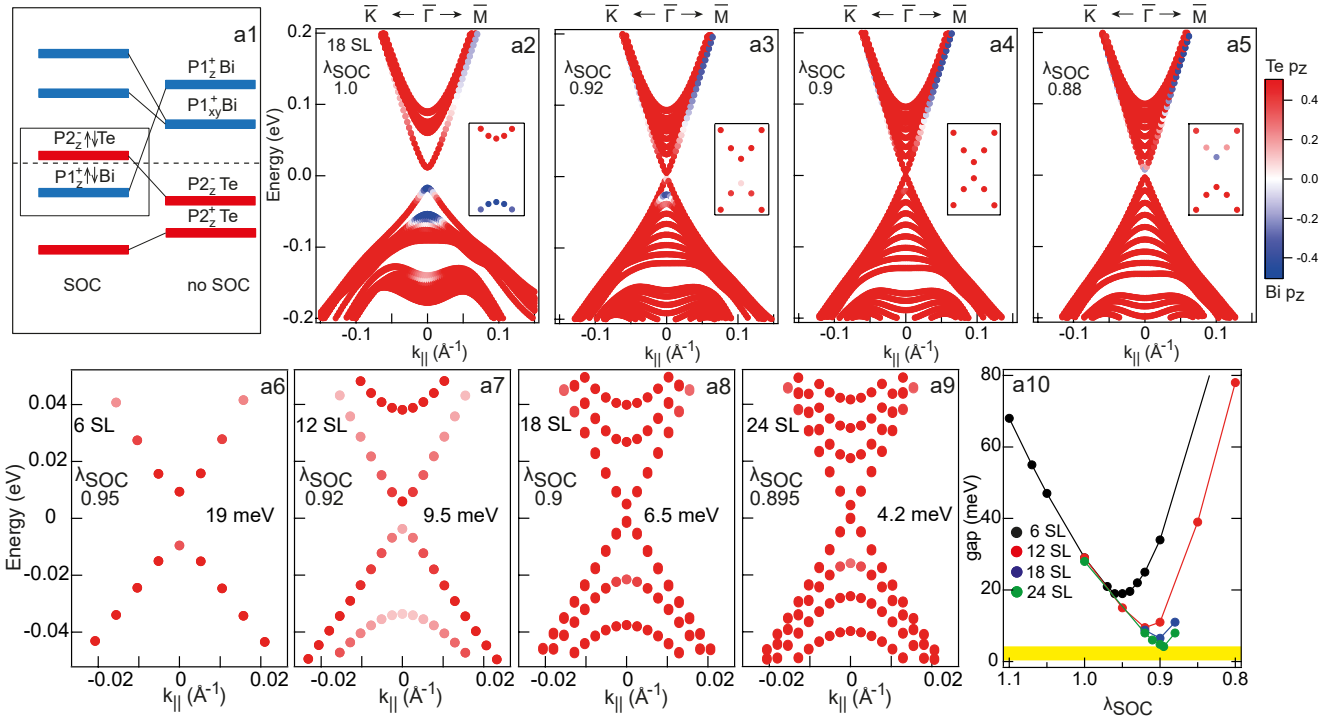

Fig. 1. (In color online) Schematic representation [26] of the inversion of the Bi p_z^+-states and the Te p_z^--states with and without SO-interaction throughout the entire bulk of the crystal (a1). Changes in the electronic structure of TSS for the 18 SLs thick slab with variation of λ_{SOC} near the minimum energy gap value at the DP (a2–a5). More detailed electronic structure of TSS at the Dirac point of the energy gap for calculated slab thicknesses of 6, 12, 18, 24 SLs (a6-a9). Corresponding changes in the energy gap value with variation of λ_{SOC} in the slab both above and below the region of minimum gap value for all calculated slab thicknesses (a10). The color scheme in the presented dispersions in Fig. a1–a5 corresponds to the difference in contributions of Te p_z^--states and the Bi p_z^+-states to the formed electronic structure. Red (blue) color corresponds to the prevalence of p_z^--state contribution (Bi p_z^+-states)

6–12 SLs, the role of correlation effects ceases to have a noticeable impact on electronic structure changes. It should be noted that changes in TSS dispersion dependence are observed only for states in the region of energy gap minimum. Meanwhile, other valence band and conduction band states are practically unaffected by slab thickness changes above 6 SLs. Here it should be noted that similar calculations performed by us for non-magnetic TI Bi_2Te_3 with calculated slab thickness of 12 SLs show that the energy gap value at the DP for this system does not exceed $2 \cdot 10^{-2}$ meV. Thus, from this comparison, it can be concluded that the minimum energy gap value for AFM TI $MnBi_2Te_4$ when passing through the TPT region has a clearly non-zero value and cannot be attributed to numerical calculation errors.

Thus, from the above, it can be concluded that with a theoretical change in the value of λ_{SOC} in AFMTI $MnBi_2Te_4$ (in a slab with thickness from 6 to 24 SLs), the system exhibits a TPT from topological to trivial state with state inversion at the edges of the energy gap at the TPT point. However, the transition does not occur with a continuous decrease in the gap value to zero at the TPT point, but with a "jump" of the Dirac gap value through zero. At the TPT point, a non-zero gap is formed, the value of which for a 24 SLs thick slab is 4.2 meV. Extrapolation of the gap value at the DP to infinite thicknesses using the available values for different slab thicknesses gives a minimum value of 3.5 meV.

It is this non-zero value of the energy gap at the TPT point that we will associate with the formation of an axion-like state at the boundary between topological and trivial phases, caused by the gradient of θ at this boundary and leading to the intercoupling of non-magnetic (SO) and magnetic contributions at the θ-boundary at the TPT point (see below).

2.2. Modification of the spin structure at the TPT point with variation of SO-coupling strength

Fig. 2 shows changes in the spin structure with spin orientation parallel (in-plane, S_x) and perpendicular (out-of-plane, S_z) to the surface, taken from work [41], with variation of λ_{SOC} in the range corresponding to TPT above ($\lambda_{SOC} = 0.95$) and below ($\lambda_{SOC} = 0.85$) the TPT point, as well as directly at the TPT point ($\lambda_{SOC} = 0.92 = \lambda_0$), calculated for a slab with thickness of 12 SLs. Figs. 2a1,b1,c1 shows spin projections S_x, and Figs. 2a2,b2,c2 shows corresponding spin projections S_z. The insets show in more detail the regions of the DP and corresponding energy gap opening at the DP. At the TPT point, the energy gap value is minimal and corresponds to 9.5 meV for this slab thickness. Red and blue symbols correspond to opposite spin orientation for both S_x- and S_z-components. The dispersion dependencies in Figs. 2a1,a2 correspond to the topological phase ($\lambda_{SOC} > \lambda_0$), and in Figs. 2c1,c2 trivial phase ($\lambda_{SOC} < \lambda_0$). Analysis shows that in all cases, the S_x-component is characterized by a helical structure (opposite signs of spin orientation for $+k_\parallel$ and $-k_\parallel$), symmetric with respect to point Γ ($k_\parallel = 0$), which is typical for TI. Such character of the spin structure persists for both topological and trivial phases near the DP. At the same time, the S_z-structure is characterized by explicit spin orientation inversion at the Γ point for the topological phase state ($\lambda_{SOC} > \lambda_0$), Figs. 2a1,a2, and absence of spin inversion in the trivial state ($\lambda_{SOC} < \lambda_0$), Figs. 2c1,c2. These changes in spin S_z-polarization indicate modulation of AFM order with variation of λ_{SOC} in the TPT region.

Figs. 2d1,d2 shows changes in TSS localization relative to the surface for values λ_{SOC} above ($\lambda_{SOC} = 1.0$) and below ($\lambda_{SOC} = 0.85$) the TPT point, calculated for a 12 SLs thick slab. The presented results show that for λ_{SOC} above the TPT point, when the system is in the TI state, the TSS are localized near the surface, and for λ_{SOC} below the TPT point, when the system is in the trivial insulator state, these states are already distributed throughout the bulk. Their localization in this case corresponds to the localization of bulk states. These changes also correspond to the system's transition from topological to trivial state.

In Fig. 2e changes in the spin S_z-polarization value for the states of the lower part of the Dirac cone in the energy gap region (blue dots in Fig. 2b2) with changes in λ_{SOC} in the TPT region are presented, showing that the maximum degree of S_z-polarization is achieved precisely in the TPT region (when approaching from the topological state side). This result indicates, on the one hand, the intercoupling between non-magnetic (SO) and magnetic interactions in the TPT region (i.e., in the region of minimal energy gap). It should be

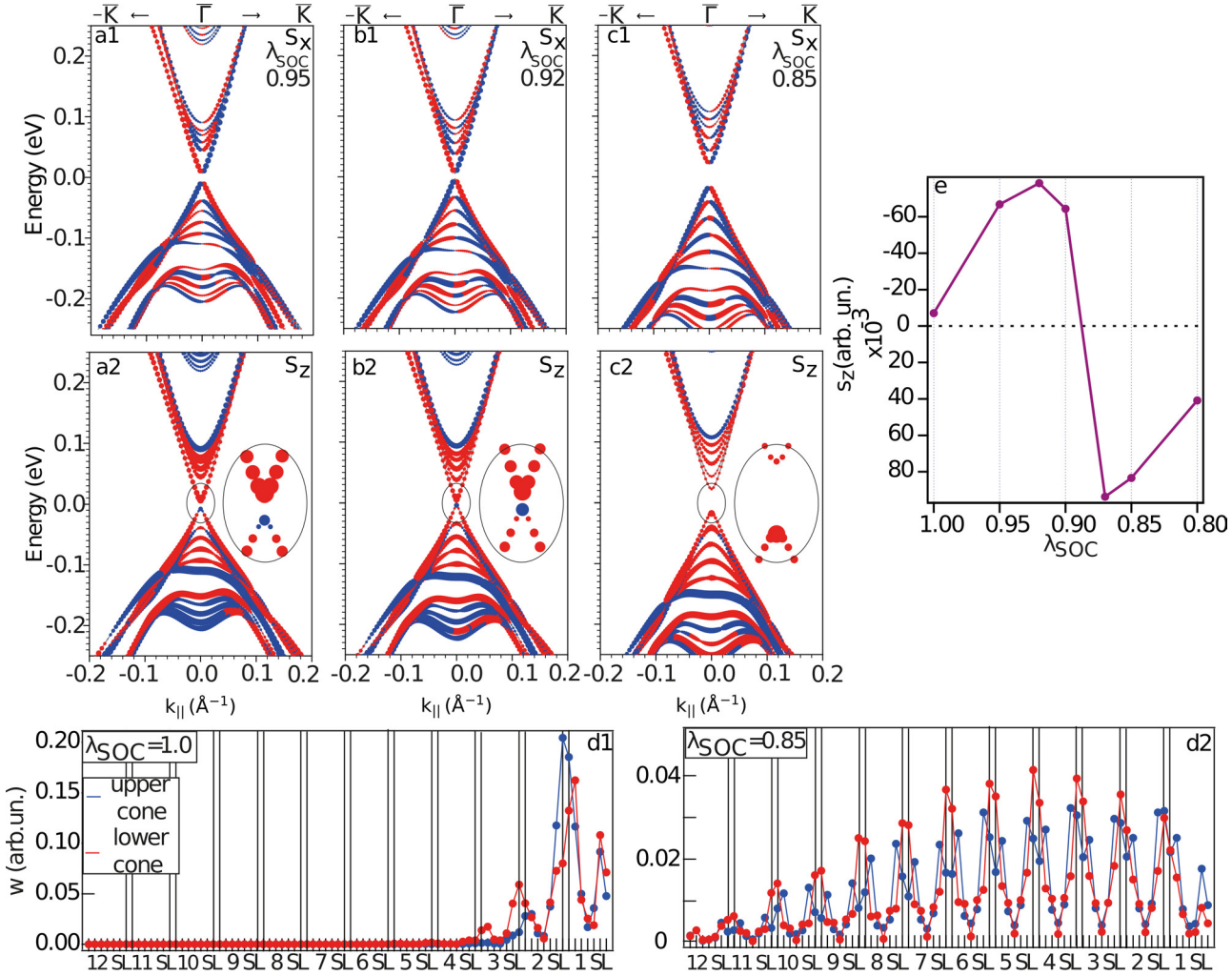

Fig. 2. (In color online) Modification of the TSS spin structure for AFM TI $MnBi_2Te_4$ with spin orientation parallel to the surface (in-plane, S_x) (a1, b1, c1) and perpendicular to the surface (out-of-plane, S_z) (a2, b2, c2), calculated for a 12 SLs thick slab in the Γ-point region for states of the upper and lower parts of the Dirac cone (red and blue points), at values of λ_{SOC} in the TPT region for cases above the transition point (a1, a2) at $\lambda_{SOC} = 0.95$; at the TPT point (b1, b2) at $\lambda_{SOC} = 0.92$ and below TPT (c1, c2) at $\lambda_{SOC} = 0.85$. The insets show a more detailed representation of the S_z-spin structure directly in the DP region. (d1, d2) – corresponding changes in TSS localization relative to the surface for values λ_{SOC} above ($\lambda_{SOC} = 1.0$) and below ($\lambda_{SOC} = 0.85$) the TPT point. (e) – change in S_z-polarization value for states of the lower part of the Dirac cone in the BG3 region of energy gap with variation of λ_{SOC} in the TPT region (from work [41])

noted that in a real system, the change in the SO-interaction strength is due to changes in the intra-atomic and surface gradients of the electrostatic potential. On the other hand, this may indicate that it is at the TPT point where this intercoupling manifests itself to the maximum degree. Thus, the minimum in the non-zero energy gap value correlates with the enhanced intercoupling between non-magnetic (SO) and magnetic interactions in the TPT region, which is an important argument in favor of the possibility of realizing an axion-like state in this system (see below).

Now it is necessary to clarify how the non-zero minimum value of energy gap at the TPT point is related to the mutual influence of non-magnetic (SO) and magnetic interactions and the change in $\theta = \pi \rightarrow 0$ in the TPT region, which is presumed to be the basis for the formation of an axion-like state at the θ-boundary between topological and trivial phases.

2.3. Connection between the minimum point of the energy gap at the Dirac point in the TPT region with the possibility of realizing an axion-like state at the θ boundary between topological and trivial phases

To summarize the results of the presented calculations, the variation (decrease) in the value

of λ_{SOC} in AFTI $MnBi_2Te_4$ is accompanied by a change (decrease) in the value of the energy gap at the DP, which reaches a minimum and then begins to increase again. At the energy gap minimum point, the system undergoes TPT from topological to trivial state. This TPT is accompanied by an inversion of the contributions of p_z^--states of Te and p_z^+-states of Bi (with different parity) at the edges of the formed energy gap at the DP, which may indicate a change in the energy gap sign, which is an indicator of TPT. At the TPT point, there is also an inversion of the spin S_z-orientation of the states of the upper and lower Dirac cones at the edges of the energy gap and a transition at the TPT point from surface localization of states forming TSS to bulk localization throughout the slab. Moreover, the value of the spin S_z-component for states of the lower part of the Dirac cone in the TPT region reaches maximum values, indicating enhanced intercoupling between non-magnetic (SO) and magnetic interactions specifically inthe TPT region.

The presented changes in the size and sign of the energy gap and their dependence on non-magnetic (SO) and magnetic interactions within the framework of the Dirac four-band model [4] correspond to changes in the values of m_4 and m_5 (see below in this section). Moreover, as calculations in this work have shown, at the TPT point, the decrease in size and sign inversion of the energy gap (determined by the size and sign of m_4 in the Dirac representation) during changes in λ_{SOC} occur not continuously but with a jump through zero. (In our calculations at the TPT point with a slab thickness of 24 SLs, the gap value at the DP was 4.2 meV). The formation of a non-zero energy gap at the TPT point in our consideration is associated with the formation of an axion-like state at the boundary between topological and trivial phases, which determines the correlation between non-magnetic and magnetic interactions at the θ-boundary between these phases. This assumption correlates with the fact that according to works [8, 10, 11, 12, 43], the point of minimum gap in the TPT region should correspond to the most effective realization of dynamic axion excitation.

It should be noted that all the above-mentioned changes at the TPT point manifest themselves precisely at the boundary between topological and trivial phases, i.e., for this system – at the boundary between crystal and vacuum (where the value of θ changes from π to 0). It is the axion field gradient at the boundary between topological and trivial phases at the TPT point (at $\theta \neq \pi$ or 0 ($\pi \to 0$)), when both time-reversal symmetry and spatial inversion are broken, that is responsible for the non-trivial correlation between non-magnetic (SO) and magnetic interactions at the θ-boundary, causing the formation of a non-zero energy gap at the TPT point, which is an indicator of the formation of an axion-like state.

This correlation can be visualized using a complex representation of the axion field $\Phi = \chi e^{i\theta}$ by introducing a change (interaction) of non-magnetic (mainly SO) and magnetic contributions (similar to works [43, 41]). The change in the strength of the SO-coupling is primarily determined by the change in the electrostatic intra-atomic potential gradient. In this case, if we consider the dependence of the energy gap value at the DP, then θ can be represented as a phase variable for the complex representation of the mass term $m = \rho e^{i\theta}$ [4, 14, 17, 43, 41], as shown in Fig. 3. The possibility of complex representation of the mass term with axion field variation was noted in the pioneering work [14]. In such representation, the real and imaginary parts can be represented as m_4 and m_5 in expression

$$m = m_4 + im_5.$$

Here

$$m_4 = \rho\cos\theta, \quad m_5 = \rho\sin\theta$$

with modulus

$$|m| = |\rho| = \sqrt{m_4^2 + (im_5)^2}.$$

The term m_4 corresponds to the contribution of non-magnetic (mainly SO) coupling in the four-band Dirac model [4, 10–12], which preserve time reversal and spatial inversion symmetry, while m_5 corresponds to the contribution of AFM-coupling (AFM-order), leading to the violation of time reversal and spatial inversion symmetry. In this representation, the topological state corresponds to the left point on the circle with radius

$$\rho = |m| = \sqrt{m_4^2 + (im_5)^2}$$

on axis m_4 (point $\theta = \pi$) in Fig. 3, which is characterized by a negative sign of the energy gap at the DP. The trivial state corresponds

to the right point on this circle (point $\theta = 0$), which is characterized by a positive sign of the energy gap.

This representation demonstrates the correlation between non-magnetic (SO) and magnetic contributions during the transition $\theta = \pi \rightarrow 0$, when the value θ differs from the quantized values π and 0, and their possible mutual transformation at the TPT point. Similar representations of the change in θ during the transition between topological and trivial phases with and without time-reversal and spatial symmetry breaking are presented in works [46, 47], which also show that this transition in the region of change θ (between quantized values π and 0, when symmetries are broken) occurs without closing the energy gap at the TPT point. In Fig. 3, this is the transition along the red arrows. For non-magnetic TI, when the transition occurs exclusively along the horizontal axis (change in m_4), where symmetry is preserved, θ transitions from value π to 0 directly at the TPT point (along a circle with zero radius). In this case, TPT occurs with zero energy gap, as shown by blue arrows.

If we theoretically decrease the value of λ_{SOC} (which corresponds to a decrease in m_4) for AFM $MnBi_2Te_4$ (in Fig. 3, this is transtition from left to right along the m_4 axis), then at λ_{SOC} values ofcorresponding to the transition region from topological to trivial state, the contributions of m_4 and m_5 become comparable (the left point on the circle in Fig. 3). In this case, the condition for preserving the combined topological invariant for $MnBi_2Te_4$ (characterized by the value $\theta = \pi$) is violated. The value of θ begins to change within between π and 0, thereby affecting the correlation between m_4 and m_5, in accordance with this complex representation, and the system transitions from the topological state ($\theta = \pi$) to the state of a trivial insulator ($\theta = 0$) with different parity and opposite sign of the energy gap at the Γ point (now with non-inverted surface states at the energy gap edges, i.e., with a positive sign of energy gap). This transition can be described by the rotation of a vector with modulus $|m|$ in this complex representation (shown by red arrows in Fig. 3). It is the invariance of the modulus $|m|$ when changing λ_{SOC} in the TPT region that determines the presence of energy gap and its invariance during such transition. In this case, the size of the energy gap corresponds to the expression

$$E_{gap} = \sqrt{m_4^2 + (im_5)^2}$$

at the TPT point (see also [10]).

A similar situation occurs when increasing the strength of the SO-coupling from small values corresponding to the trivial phase (starting from the right point in the complex representation in Fig. 3). In this case, this correlation manifests itself explicitly only when exceeding a certain threshold of the intra-atomic potential gradient (i.e., in the TPT region).

It should be noted that in accordance with the Gauss's law with the introduced axion term [4, 14, 48–50]

$$\nabla \cdot \mathbf{E} = \rho - \frac{\alpha}{4\pi^2} \nabla\theta \cdot \mathbf{B},$$

it is the gradient θ at the boundary between topological and trivial phases that causes the corresponding correlation between electric and magnetic fields (or SO (m_4) and magnetic (m_5) contributions) at the θ-boundary in the TPT region, which leads to the formation of an axion-like state at the boundary between topological and trivial

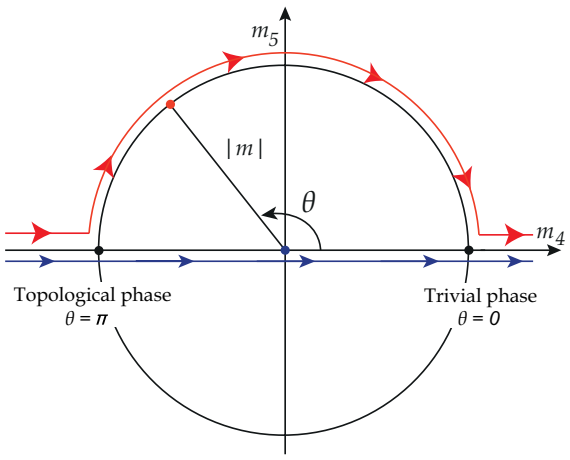

Fig. 3. (In color online) Schematic complex representation of the correlation between the axion field θ and non-magnetic order, described by the value m_4 (mainly due to SO-coupling), and AFM order, described by m_5, in the TPT region within the range of $\theta = \pi \rightarrow 0$. Here, the topological state corresponds to the left point on the circle (with radius $\rho = \sqrt{m_4^2 + (im_5)^2}$ on the axis m_4 ($\theta = \pi$)), which is characterized by a negative energy gap ($m_4 < 0$). The trivial state corresponds to the right point of the circle ($\theta = 0$), which is characterized by a positive sign of energy gap at the DP ($m_4 > 0$). For AFM TI $MnBi_2Te_4$, the transition from topological to trivial state occurs along the circle's radius, shown by red arrows (without closing the energy gap). For non-magnetic TIs, the topological transition occurs along the axis m_4 (at $m_5 = 0$) without opening the energy gap, shown by blue arrows (from work [41])

media, which manifests itself, among other things, in the formation of a non-zero energy gap at the DP during TPT and the corresponding topological ME effect (for a system with parameters close to TPT). Such representation somewhat correlates with the axion instability effect analyzed in works [43, 51, 52]. Within this effect, when the electric field applied to the system exceeds a certain level E_{crit}, the electric field begins to be screened, which leads to the emergence of local magnetic flux density in the region of the θ-boundary due to the ME effect [43]

$$B(\theta) = 4\pi\mu M_{\theta} = \frac{\alpha}{\pi}\mu\theta E(\theta).$$

In other words, the axion instability effect can also be considered as an effect of unique correlation between electric and magnetic fields in the region of θ change.

2.4. Modulation of electronic and spin structures under applied electric field for a system based on AFM TI $MnBi_2Te_4$ with parameters corresponding to TPT

Interestingly, if an electric field is applied perpendicular to the surface (or external gradient of electrostatic potential) for a system based on AFM TI $MnBi_2Te_4$, characterized by the value λ_{SOC} in the TPT region, then depending on the polarity of the applied electric field (gradient direction), this will lead to the transformation of the system either into topological or trivial phase.

Fig. 4 (as a further development of ideas presented in works [41, 43]) shows changes in S_z-spin structure with detailed spin-dependent dispersion relations of TSS in the DP region when applying external potential gradient by introducing "vacuum-slab-metal" boundary conditions into calculations with additional charge in the system [53], which is parametrically in the TPT region ($\lambda_{SOC} = 0.92$). Red and blue symbols correspond to opposite spin orientations. Calculations were performed for a slab with thickness of 12 SL. Quantitative changes in S_z for states of the lower part of the Dirac cone under applied electric field of opposite polarity for different values of applied field gradient relative to TPT point ($\lambda_{SOC} = 0.92$) are shown in Fig. 4b. The analysis shows that when applying a field of positive polarity, the out-of-plane spin S_z-component at the DP shows clearly increasing degree of spin S_z-polarization, corresponding to system transition into topological state, with spin S_z-polarization even greater than for topological phase without applied electric field. On the other hand, when applying field

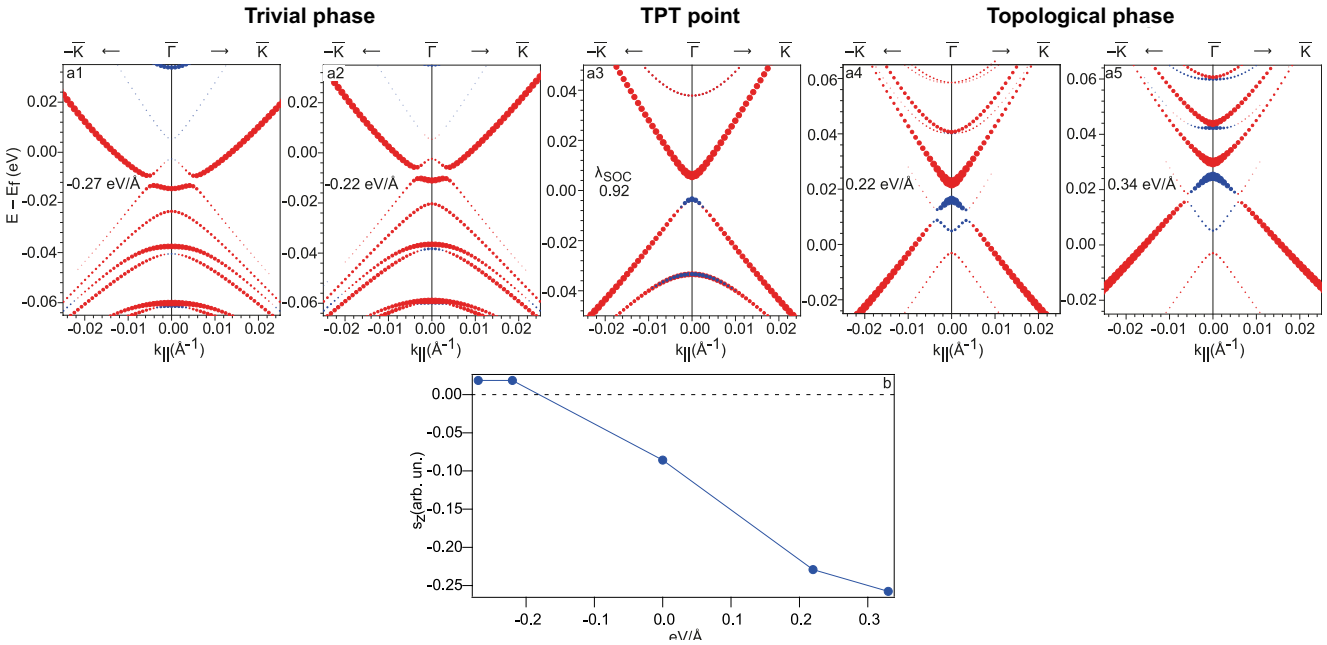

Fig. 4. (In color online) (a1–a5) – Changes in out-of-plane (S_z) spin structure with detailed dispersion relations of TSS in DP region under applied electric field (perpendicular to surface) of opposite polarity relative to the system parametrically in TPT region ($\lambda_{SOC} = 0.92$). Applied field strength values are shown in corresponding insets. Red and blue symbols correspond to opposite spin orientations. Calculations were performed for a slab with thickness of 12 SLs. (b) – Changes in the S_z value for states of the lower part of Dirac cone under applied electric field of opposite polarity for different values of applied field gradient relative to TPT point ($\lambda_{SOC} = 0.92$)

of negative polarity, the system transitions to trivial state without corresponding inversion of spin states at the edges of energy gap at the DP.

The results of these calculations show that, on the one hand, for a system with parameters in the TPT region, it is easy to switch the system from topological to trivial state and vice versa by applying an electric field of opposite direction perpendicular to the surface, i.e., to control the TPT. On the other hand, these calculations show the correlation between electrical and magnetic couplings in the TPT region. The electric field applied perpendicular to the surface causes an out-of-plane (S_z) spin polarization, indicating the formation of a local magnetic field perpendicular to the surface, which corresponds to the possibility of realizing the topological ME effect in the TPT region.

3. CONCLUSION

To analyze the possibility of implementing TPT and the connection of this transition with the formation of an axion-like state localized at the boundary between topological and trivial phases, comparative calculations and analysis of changes in electronic and spin structures in systems based on AFM TI $MnBi_2Te_4$ in slabs of various thicknesses (6, 12, 18, 24 SLs) were performed using density functional theory, with variation of the strength of the SO-coupling in the TPT region between topological and trivial states of the system.

The calculations showed that at the TPT point, the value of the energy gap reaches its minimum with decreasing value λ_{SOC} (for a 24 SLs thick slab, the minimum energy gap is 4.2 meV), and then after passing through the TPT point with further decrease in λ_{SOC} it begins to increase again during the transition to the trivial state. Simultaneously, at the TPT point, there is an inversion of contributions from p_z^+-states of Bi and p_z^--states of Te with different parity at the edges of the energy gap, which occurs in the TPT point region, indicating an inversion of the formed energy gap sign. At the TPT point, there is an inversion of the out-of-plane (S_z) spin polarization at the point Γ for the states of the lower and upper parts of the Dirac cone.

The transition from a topological to a trivial state of the system when changing λ_{SOC} occurs without closing the energy gap, i.e., with a "jump" through 0 and formation of a non-zero energy gap during such transition, which indicates the intercoupling of non-magnetic electrical (SO) and magnetic couplings in the TPT region and the formation of an axion-like state at the θ-boundary between topological and trivial phases.

In this case, it is the gradient of θ ($\theta = \pi \to 0$) at the boundary between topological and trivial media that causes a non-trivial intercoupling between non-magnetic (SO) and magnetic couplings at the θ-boundary at the TPT point, i.e., the formation of an axion-like state, which manifests itself, among other things, in the formation of a non-zero Dirac energy gap during TPT.

A comprehensive representation of such intercoupling is proposed for values of λ_{SOC} corresponding to the TPT region, at the θ-boundary, where the axion term varies between quantized values ranging from π to 0. At the TPT point, the system transitions from a topological state ($\theta = \pi$) to a trivial insulating state ($\theta = 0$) with different parity and opposite sign of energy gap at the Γ point through mutual transformation between electric and magnetic contributions within the range of $\theta = \pi \to 0$, which determines the non-zero energy gap during TPT.

Application of an electric field perpendicular to the surface of a system based on AFM TI $MnBi_2Te_4$, with parameters close to the TPT state, allows controlling the transition from topological to trivial state and vice versa when changing the direction of the applied electric field, which shows the intercoupling of electric and magnetic contributions in the TPT region and the possibility of implementing a topological ME effect in the TPT region.

4. METHODS

Electronic structure calculations were performed using the OpenMX software code, which implements a fully relativistic density functional theory method using norm-conserving pseudopotentials [54] and pseudo-atomic orbitals as basis functions [55–57]. The calculations were carried out within the generalized gradient approximation using its PBE version [58]. The integration grid in real

space was determined by the cutoff energy of 450 Ry, and in reciprocal space, for the Brillouin zone sampling, the grid was set as 5×5×5 k-points for bulk crystal calculations and 5×5×1 k-points if a surface was present. Testing showed that further increase in k-grid density leads only to very weak changes in the electronic structure. The convergence criterion for total energy was set to $1 \cdot 10^{-6}$ eV. The basis functions were defined as follows: Bi8.0-$s3p2d2f1$, Te7.0-$s3p2d2f1$, Mn6.0-$s3p2d1$. The Mn3d states were treated within the DFT $+U$ [59] approach using Dudarev's scheme with parameter $U = 5.4$ eV [23]. The surface computational cell $MnBi_2Te_4$ included a vacuum layer of 12 Å thickness. The external gradient of electrostatic potential along the surface normal was set by placing an electric charge on one side of the slab using the effective screening medium method [53] with "vacuum-slab-metal" boundary conditions

FUNDING

The work was carried out within and supported by the Russian Science Foundation (grant No. 23-12-00016) and Saint Petersburg State University (grant No. 94031444).

REFERENCES

1. X.-L. Qi, T. L. Hughes, and S.-C. Zhang, Phys. Rev. B 78, 195424 (2008).

2. X.-L. Qi and S.-C. Zhang, Rev. Mod. Phys. 83, 1057 (2011).

3. D. M. Nenno, C. A. C. Garcia, J. Gooth et al., Nature Rev. Phys. 2, 682 (2020).

4. A. Sekine and K. Nomura, J. Appl. Phys. 129, 141101 (2021).

5. C.-Z. Chang, C.-X. Liu, and A. H. MacDonald, Rev. Mod. Phys. 95, 011002 (2023).

6. A. Essin, J. Moore, and D. Vanderbilt, Phys. Rev. Lett. 102, 146805 (2009).

7. Y. Zhao and Q. Liu, Appl. Phys. Lett. 119, 060502 (2021).

8. R. Li, J. Wang, X.-L. Qi et al., Nature Phys. 6, 284 (2010).

9. Y. Xiao, H. Wang, D. Wang et al., Phys. Rev. B 104, 115147 (2021).

10. T. Zhu, H. Wang, H. Zhang et al., npj Comput. Mat. 7, 121 (2021).

11. H. Wang, D. Wang, Z. Yang et al., Phys. Rev. B 101, 081109 (2020).

12. J. Zhang, D. Wang, M. Shi et al., Chinese Phys. Lett. 37, 077304 (2020).

13. R. D. Peccei and H. R. Quinn, Phys. Rev. Lett. 38, 1440 (1977).

14. F. Wilczek, Phys. Rev. Lett. 58, 1799 (1987).

15. N.V. Mikheev and L.A. Vassilevskaya, Phys. Lett. B 410, 203 (1997).

16. J. Preskill, M. B. Wise, and F. Wilczek, Phys. Lett. B 120, 127 (1983).

17. L. D. Duffy and K. van Bibber, New J. Phys. 11, 105008 (2009).

18. F. Chadha-Day, J. Ellis, and D. J. E. Marsh, Sci. Adv. 8, eabj3618 (2022).

19. J. Wang, B. Lian, X.-L. Qi, and S.-C. Zhang, Phys. Rev. B 92, 081107 (2015).

20. T. Morimoto, A. Furusaki, and N. Nagaosa, Phys. Rev. B 92, 085113 (2015).

21. M. Mogi, M. Kawamura, R. Yoshimi et al., Nature Mater. 16, 516 (2017).

22. M. Mogi, M. Kawamura, A. Tsukazaki et al., Sci. Adv. 3, eaao1669 (2017).

23. M. M. Otrokov, I. I. Klimovskikh, H. Bentmann et al., Nature 576, 416 (2019).

24. Z. S. Aliev, I. R. Amiraslanov, D. I. Nasonova et al., J. Alloys Comp. 789, 443 (2019).

25. J. Li, Y. Li, S. Du et al., Sci. Adv. 5, eaaw5685 (2019).

26. D. Zhang, M. Shi, T. Zhu et al., Phys. Rev. Lett. 122, 206401 (2019).

27. Y. Gong, J. Guo, J. Li et al., Chin. Phys. Lett. 36, 076801 (2019).

28. D. A. Estyunin, I. I. Klimovskikh, A. M. Shikin et al., APL Mater. 8, 021105 (2020).

29. A. M. Shikin, D. A. Estyunin, N. L. Zaitsev et al., Phys. Rev. B 104, 115168 (2021).

30. A. M. Shikin, D. A. Estyunin, I. I. Klimovskikh et al., Scient. Rep. 10, 13226 (2020).

31. A. M. Shikin, D. A. Estyunin, N. L. Zaitsev et al., JETP 134, 103 (2022).

32. M. Garnica, M. M. Otrokov, P. C. Aguilar et al., npj Quant. Mater. 7, 7 (2022).

33. S. V. Eremeev, M. M. Otrokov, A. Ernst et al., Phys. Rev. B 105, 195105 (2022).

34. A. M. Shikin, T. P. Makarova, A. V. Eryzhenkov et al., Physica B 649, 414443 (2023).

35. Y.-J. Hao, P. Liu, Y. Feng et al., Phys. Rev. X 9, 041038 (2019).

36. Y. J. Chen, L. X. Xu, J. H. Li et al., Phys. Rev. X 9, 041040 (2019).

37. P. Swatek, Y. Wu, L.-L. Wang et al., Phys. Rev. B 101, 161109 (2020).

38. S. V. Eremeev, I. P. Rusinov, Yu. M. Koroteev et al., J. Phys. Chem. Lett. 12, 4268 (2021).

39. H. Zhang, W. Yang, Y. Wang et al., Phys. Rev. B 103, 094433 (2021).

40. L. Zhou, Z. Tan, D. Yan et al., Phys. Rev. B 102, 085114 (2020).

41. A. M. Shikin, T. P. Estyunina, A. V. Eryzhenkov et al., Sci. Rep. 13, 16343 (2023).

42. V. A. Volkov and V. V. Enaldiev, JETP 149, 702 (2016) [V. A. Volkov and V. V. Enaldiev, JETP 122, 608 (2016)].

43. T. Imaeda, Y. Kawaguchi, Y. Tanaka et al., J. Phys. Soc. Jpn 88, 024402 (2019).

44. M. M. Otrokov, I. P. Rusinov, M. Blanco-Rey et al., Phys. Rev. Lett. 122, 107202 (2019).

45. Y. Li, Y. Jiang, J. Zhang et al., Phys. Rev. B 102, 121107 (2020).

46. S. Coh, D. Vanderbilt, A. Malashevich et al., Phys. Rev. B 83, 085108 (2011).

47. N. P. Armitage and L. Wu, SciPost Phys. 6, 046 (2019).

48. G. Rosenberg and M. Franz, Phys. Rev. B 82, 035105 (2010).

49. N. Yamamoto, Phys. Rev. D 93, 085036 (2016).

50. F. S. Nogueira, Z. Nussinov, and J. van den Brink, Phys. Rev. D 94, 085003 (2016).

51. J. Wang, B. Lian, and S.-C. Zhang, Phys. Rev. B 93, 045115 (2016).

52. H. Ooguri and M. Oshikawa, Phys. Rev. Lett. 108, 161803 (2012).

53. M. Otani and O. Sugino, Phys. Rev. B 73, 115407 (2006).

54. N. Troullier and J. Martins, Phys. Rev. B 43, 1993 (1991).

55. T. Ozaki, Phys. Rev. B 67, 155108 (2003).

56. T. Ozaki and H. Kino, Phys. Rev. B 69, 195113 (2004).

57. T. Ozaki and H. Kino, Phys. Rev. B 72, 045121 (2005).

58. J. P. Perdew, K. Burke, and M. Ernzerhof, Phys. Rev. Lett. 77, 3865 (1996).

59. M. J. Han, T. Ozaki, and J. Yu, Phys. Rev. B 73, 045110 (2006).